Fuel 294 (2021) 120468

Contents lists available at ScienceDirect

Fuel

journal homepage: www.elsevier.com/locate/fuel

Full Length Article

The effects of injector geometry and operating conditions on spray mass, momentum and development using high-pressure gasoline

M. Medina [a,*], A. Bautista [b], M. Wooldridge [c], R. Payri [b]

[a] Department of Mechanical Engineering, University of Michigan, United States
[b] CMT - Motores Termicos, Universitat Politecnica de Valencia, Valencia, Spain
[c] Department of Mechanical Engineering, University of Michigan, United States

ARTICLE INFO

Keywords:
High-pressure gasoline
Cavitation
Schlieren imaging
Hydraulic characterization
Injector temperature
Internal geometry

ABSTRACT

High fuel injection pressure (>500 bar) in direct injection gasoline engines is an important means to reduce particulate emissions. While decades of fuel spray research has dramatically advanced the understanding high-pressure diesel fuel sprays, few studies focus on high-pressure gasoline sprays. The objective of this work was to quantify the effects of different injector nozzle geometries on important high-pressure gasoline spray characteristics including injection mass flow rate, momentum flux, and spray imaging at evaporative and non-evaporative conditions. Three categories of nozzle internal geometry were evaluated: inlet rounding; converging-, diverging-, and straight-cylindrical internal flow passages; and different nozzle outlet diameters. Reference grade gasoline was used at injection pressures of 600, 900, 1200, and 1500 bar at chamber pressures from 1 to 30 bar and chamber temperatures from 293 to 800 K. Two fuel injector temperatures of 293 K and 363 K were studied. The mass and momentum measurements were used to quantify differences in injector geometry as well as to evaluate for effects of cavitation. The visualization data were analyzed to determine spray penetration and spray angle development for a broad range of operating and state conditions. The results showed internal flow significantly impacts injector performance, where nozzles with inlet rounding resulted in 20% higher mass flow rate compared with straight cylindrical nozzles. Higher fuel injector temperatures also increased mass flow rate by up to 5%. Spray momentum coefficients showed a linear relationship with cavitation number indicating all nozzles were cavitating at all conditions tested. Trends in fuel spray penetration and spray angle development were similar to those observed previously for diesel sprays, which was unexpected given the significant differences in thermal-physical properties of the fuels. Chamber pressure had the strongest influence on penetration distance, and the momentum measurements were good indicators of the injector geometry with the highest penetration distance.

1. Introduction

Fuel spray research has advanced dramatically over the past three decades with respect to diesel sprays. Particularly, our understanding of diesel combustion [1], predictions of diesel fuel spray characteristics with semi-empirical correlations [2–4] and effects of operating conditions and injector geometry on diesel fuel spray behavior such as droplet distribution, Sauter Mean Diameter, cavitation, liquid length, cycle-to-cycle variability, apparent heat release, etc. [5–10]. Recent advancements in gasoline direct injection (GDI) engines and gasoline compression ignitions (GCI) concepts among other combustion strategies have focused on improving the gasoline fuel injection process [11–13]. However, few previous studies have considered high fuel injection pressures (specifically injections pressures higher than 500 bar) for gasoline, and fewer have considered the early times of the spray development (i.e., transition between momentum and diffusion flow). High fuel injection pressures are of interest due the benefits observed with improved fuel atomization as injection pressure increases [14,15]. It is important to know the potential issues and benefits associated with high gasoline fuel injection pressures. Additionally, multiple fuel injection events per cycle offer unprecedented levels of control of mixture stratification/homogeneity and are routinely used with GDI engines to improve engine performance and lower engine-out emissions [16–18]. Thus, a broad range of back-pressures (i.e., combustion chamber pressures) and temperatures are important for consideration in spray studies and relevant to GCI and GDI engines.

* Corresponding author at: Department of Mechanical Engineering, California State University, Los Angeles, United States.

https://doi.org/10.1016/j.fuel.2021.120468
Received 10 December 2020; Received in revised form 6 February 2021; Accepted 9 February 2021
Available online 8 March 2021

The previous studies of high-pressure gasoline fuel sprays are briefly summarized here. In the study by Kim et al. [19], the authors compared diesel and gasoline fuel spray development at fuel injection pressures between 400 and 1000 bar at two bar chamber pressure in a constant volume chamber (CVC). The CVC results showed gasoline yielded a shorter liquid penetration length compared with diesel fuel, but the gasoline sprays produced larger spray cone angles. Kim et al. [19] also performed engine studies using an optically-accessible single-cylinder engine and qualitatively compared the spray development of the two fuels at injection pressures of 400 and 600 bar. The engine results showed that under evaporating conditions the penetration of gasoline was significantly lower than for diesel. Both fuels yielded comparable peak indicated mean effective pressure, but gasoline combustion resulted in lower NOx emissions.

Unlike the study by Kim et al. [19], the study by Payri et al. [20] showed the penetration distances of diesel and gasoline sprays were similar at fuel injection pressures between 600 and 1500 bar in a CVC under non-evaporating conditions. Payri et al. proposed the mixing processes for diesel and gasoline at non-evaporative conditions were the same based on the similar penetration distance and momentum flux measurements for both fuels.

Tian et al. [21] derived a semi-empirical correlation for the penetration distance of high-pressure gasoline sprays based on their experimental study of p-xylene sprays in a CVC at non-evaporating conditions (300 K) and evaporating conditions (500–760 K). Tian et al. [21] compared spray penetration data at injection pressures between 200 and 1200 bar at a chamber pressure of one bar (for non-evaporative conditions) and 10 to 40 bar (for evaporative conditions). The correlation for penetration distance as a function of time used parameters found in previous diesel spray correlations, including the difference between the fuel injection pressure and the chamber pressure, nozzle outlet diameter, fuel density, and ambient density, and the authors included ambient temperature as a means to include vaporization effects. Importantly, the correlation by Tian et al. [21] did not propose a spray break-up time, which has been widely used for diesel spray correlations. The correlation was compared with experimental results for high-pressure gasoline sprays in the study by Medina et al. [22]. The comparisons showed significant discrepancies at all times, which may be due to the lack of a transition in spray development, i.e., omission of a spray break-up time in their model.

The recent study by Yamaguchi et al. [15] included spray studies using n-heptane and various nozzle geometries at pressures up to 1500 bar. The authors found divergent nozzles produced shorter penetration than convergent nozzles. Using droplet size measurements, they also concluded increased injection pressure yields smaller droplets with the most pronounced decrease at injection pressures of 800 bar. Given the study was conducted using n-heptane, it would be valuable to confirm if the trends observed are consistent for multi-component gasoline.

In addition to fuel effects, experimental data for high-pressure gasoline sprays at broader operating conditions are needed to guide engine development, to advance spray theory, and to resolve discrepancies in existing data. Based on this need, the objective of the current study was to systematically quantify high-pressure gasoline fuel spray development including the effects of different internal nozzle geometries with a range of high-fidelity diagnostics. This work expands on our previous high-speed imaging studies of high-pressure gasoline fuel sprays [22,23] to include new measurements of injection rates and momentum flux and to include the effects of injector temperature. The additional characterization allows important new analysis and interpretation of the sprays, including consideration of the effects of cavitation.

2. Experimental methodology

In this study, two multi-hole prototype research grade fuel injectors were studied in three experimental facilities. The injector bodies were production diesel hardware. The key features of the internal geometry of each orifice are provided in Table 1. Further details are discussed in Medina et al. [23]. Two experimental facilities were used to measure the time-resolved mass flow rate and the time resolved momentum of the sprays. A high-temperature and high-pressure facility was used to visualize the external spray development using high-speed schlieren imaging. The fuel properties of the reference grade gasoline (Total, SP S98S V2005) used in the study are listed in Table A1 of the Appendix. For each of the measurements, the fuel was pressurized using a custom piston pump and supplied to the injector through a common rail system. Injection events were electronically controlled using an impulse generator (Genotec). The energize time for all injection events was set to 1 ms, similar to the experiments conducted in Medina et al. [22,23], to simulate typical gasoline direct injection performance and to represent transient injector behavior. It is important to note using a constant injection duration leads to different amounts of fuel mass injected for different fuel injection pressures. Consequently, the interpretation and discussion of the results considers the effects of changing fuel mass for conditions with different fuel injection pressures.

2.1. Instantaneous mass flow rate characterization

A commercially available injection rate discharge curve indicator (IRDCI) (IAV, type N-050–028) , which employs the Bosch method [24], was used to measure the instantaneous mass flow rate of the sprays from the injectors, i.e., the rate of injection (ROI). The IRDCI consists of a pressure sensor, a long fuel-filled tube, a large fuel reservoir, a relief valve, and a back-pressure cavity typically filled with nitrogen to reduce pressure oscillations. A schematic of the IRDCI is shown in Figure A1 of the Appendix. Details on the fundamental working principle are provided in previous studies [24–26]. The functionality of the facility is briefly described here. Fuel is injected into the long fuel-filled tube at the start of the test. The fuel injection event produces a pressure wave that is proportional to the instantaneous mass flow rate. The pressure wave is detected using a fast-response piezoelectric pressure sensor. The underlying theory is based on the hydraulic pulse theorem [24–26]. To account for uncertainties in the measurement related to the speed of sound, fuel is collected at the outlet of the IRDCI at the same rate at which fuel is being added to the reservoir. The fuel is collected on a mass balance, serving as a second mass flow rate measurement and for comparison with the IRDCI pressure-based measurements. The experimental error associated with the IRDCI measurements of fuel mass flow rate is less than 0.6% [26,27].

For each IRDCI experiment, the injector is placed in a cooling jacket that is fixed at the entrance of the IRDCI. The cooling jacket provides a continuous flow of temperature-controlled coolant, and thus the injector temperature is considered the same as the coolant temperature Four injection pressures, three chamber pressures, and two coolant temperatures were tested and are listed in Table 2. Two sets of data with 50 repetitions each were collected at each condition. The first data set was used to verify stability and repeatability, and the second data set was used for analysis.

2.2. Instantaneous momentum characterization

The momentum rate meter is a custom-designed enclosed vessel with high-pressure chamber capabilities and optical access. The underlying assumptions and details of the system are presented in previous studies [28]. A schematic of the spray momentum rate meter is provided in Fig. A2 of the Appendix. A brief summary of the operation is provided here. For a typical experiment, the chamber is pressurized with nitrogen to conditions consistent with the injection timing in a piston engine of interest. Momentum measurements are acquired using a piezoelectric sensor aligned perpendicular to the axis of the fuel spray. Only one spray plume is allowed to impact the sensor in the tests. The impact force of the spray plume is directly related to the axial momentum flux of the spray.

Table 1
Injector nozzle characteristics.

Injector	Orifice No.	Normalized outlet diameter*	Conicity of nozzle passage**	Hydro-erosion rounding of nozzle inlet	L/d Ratio†	Schematic of nozzle cross-section
X	Hole 1	0.578	0	0%	8.2	
	Hole 2	1	0	0%	4.7	
Y	Hole 1	0.789	−1.5	20%	6	
	Hole 2	0.789	3.5	20%	6	

Table 2
Summary of experimental conditions.

Parameter	Facility		
	IRDCI	Momentum Flux	CPF Reactor
Chamber gas	–	Nitrogen	Nitrogen
Fuel type	Reference grade gasoline		
Injector Tested	X and Y (see Table 1)		
Injection Pressures [bar]	600, 900, 1200, 1500		
Chamber Pressure [bar]	10, 20 30	5, 10, 20, 30	5, 10, 20, 30
Chamber Temperature [K]	293	293	400, 600, 800
Coolant Temperature [K]	293, 363	363	293, 363
Number of repetitions	100	100	20

For the current work, the sensor target area was placed 8 mm from the nozzle outlet. This was the minimum distance to ensure no interference between the two plumes. This small distance also avoids potential losses from the spray due to atomization and evaporation. Similar to the IRDCI tests, two data sets of 50 measurements each were recorded. Four fuel injection pressures, four chamber pressures, and one coolant temperature were tested. The complete list of conditions is provided in Table 2.

2.3. High-speed imaging characterization

A custom-designed, high-temperature, high-pressure test facility was used to image the gasoline spray development. A detailed description of the facility is presented in Payri et al. [29]. A brief summary of the facility and the experimental approach is provided here. The facility is a constant-pressure flow (CPF) reactor with the ability to create nearly quiescent and steady thermodynamic conditions [30]. During an experiment, the chamber is continuously pressurized with nitrogen to simulate engine conditions and has three orthogonal optical access ports each with viewing access of 12.8 cm. The chamber is rated to a maximum temperature of 1000 K and a maximum pressure of 150 bar. A schematic of the CPF reactor is provided in Figure A3 of the Appendix. The operating conditions used in the reactor experiments are listed in Table 2.

Schlieren imaging has been used extensively to visualize spray development [10,31–33]. The imaging technique used in this study was a single pass schlieren setup. A schematic of the optical arrangement is shown Figure A4 of the Appendix. The technique consists of a light source, collimating mirror, focusing lens, diaphragm, and camera. The light from a mercury-xenon arc lamp is passed through a pin-hole with a diameter of 1.2 mm. The light is reflected from a 150 mm parabolic mirror with a focal length of 650 mm, collimating the light through the test section. After passing through the test section, the light is focused with a 150 mm biconvex lens onto a diaphragm placed at the focal point of 450 mm. The diaphragm is set to a diameter of 4 mm and in front of the high-speed camera (Photron Fastcam SA5). The images were recorded using a 100 mm lens (Zeiss) with the camera and the camera settings are listed in Table A2 of the Appendix.

2.4. Data processing

The data collected in the three facilities were processed using methods specific to each experimental approach. Details are provided in references [27,28,32,34], and the approaches are briefly summarized here.

The IRDCI data from all 50 injection events were averaged and converted to mass flow rates/ROI, including corrections for signal bias, using the methods described in Bosch et al. [24], and Payri et al. [27]. The ROI data were then integrated to obtain the total injected mass. The calculated mass was compared with the measurement from the mass balance. Using both measurements, a scaling factor was determined and used to correct the IRDCI measurements. An example of the corrected ROI signal is shown in Fig. 1 along with the integrated mass, indicated by the shaded area. For each time-history of mass flow rate, a region was selected for analysis after the start of injection and before the end of injection, where the injection rate was relatively stable as a function of time and consistent across all injection events. For this study, the region used for the calculation for all injection events was characterized by the two peaks shown with dashed lines in Fig. 1. The ROI data in this region were mathematically averaged and identified as the characteristic injection rate for each experiment. The ROI data were then used to calculate hydraulic coefficients such as the momentum coefficient and discharge coefficient for each injector. Variability in the time interval selected for analysis was considered in the uncertainty of the hydraulic coefficients determined from the data.

The characteristic momentum flux values were determined using similar methods as used to determine the characteristic ROI. A time region with consistent behavior was used to determine the average momentum flux for each operating condition. Fig. 2 shows an example of the momentum flux measurement where the stabilized range is indicated with vertical dashed lines. The uncertainty in the

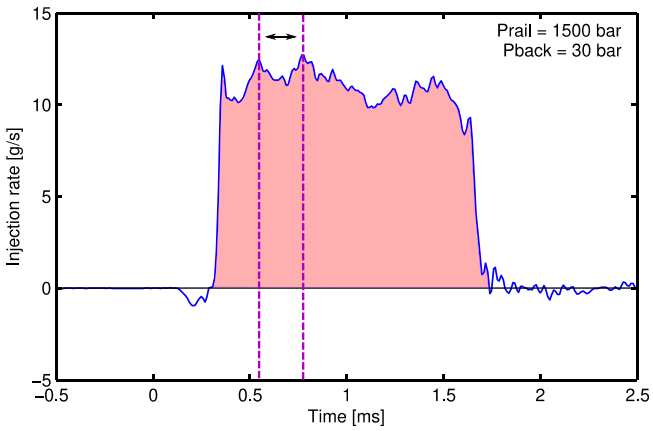

Fig. 1. Rate of injection (ROI) results for 1500 bar injection pressure and 30 bar back pressure for Injector Y. The data include the mass from both nozzle holes of the injector. The shading represents the total mass per injection event. The vertical dashed lines indicate the region of the ROI data used as the characteristic injection rate.

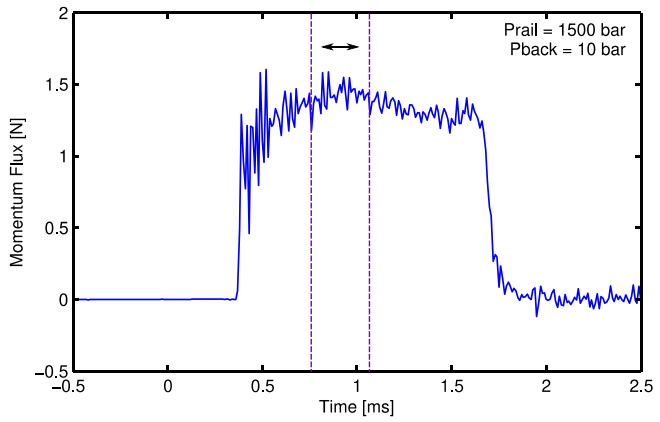

Fig. 2. Momentum flux measurement for 1500 bar injection pressure and 10 bar chamber pressure. The vertical dashed lines indicate the stabilized region used to determine the average momentum flux for the operating condition.

characteristic momentum flux values reported here is ± 2% and is primarily due to the variability in the time interval selected.

The high-speed schlieren images were used to quantify the spray development in terms of spray tip penetration and spray angle. The image processing included four major steps: image masking, background subtraction, contour detection, and contour analysis. Figures showing intermediate results of the image analysis are provided in the Appendix (Fig. A5). Image masking was determined by defining the general area where the sprays were located using the centerline axis of the sprays and the maximum anticipated width of the spray, creating a segmented triangular shape. To perform accurate background subtraction, two algorithms were implemented: dynamic background subtraction and image temporal derivative [32,33]. The algorithms are complementary because the dynamic background captures a majority of the dense regions of the spray and the image temporal derivative captures the dilute fluid regions. Once each spray was isolated, contour detection was performed using binary images. Spray tip penetration distance and spray angle were calculated for each time step using the contours from the binary images. A typical processed image is shown in Fig. 3 along with examples of measurements of penetration distance (defined as the farthest point of the spray from the center of the nozzle hole) and spray angle (defined as the angle at one-third the penetration distance of the spray). Additional details on the image processing algorithms can be found in the literature [6,32,33]. The uncertainty in the penetration distance and the spray angle was 0.5% and 1.5%, respectively, and is primarily due to the parameters used in the image processing, e.g., the threshold applied to create the binary images.

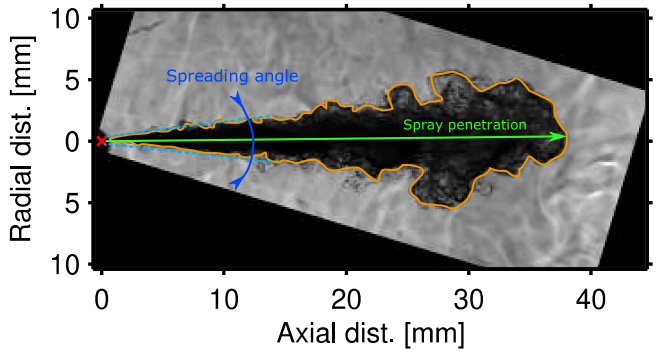

Fig. 3. Typical processed image of spray with plume contour shown in orange, spray tip penetration shown in green, and spray angle shown in blue. (For interpretation of the references to colour in this figure legend, the reader is referred to the web version of this article.)

3. Results

The experimental matrix of the study spanned a wide range of operating conditions and four nozzle geometries in the three facilities. In the interest of conciseness, representative data are presented in the following sections. The results at other conditions followed similar trends unless specified otherwise. The additional data from the different facilities and experimental conditions are presented in the Appendix for reference.

4. Mass flow rate

Fig. 4 shows the injection rate results for two coolant temperatures (20 °C and 90 °C) for Injector Y at 1500 bar injection pressure and 20 bar chamber pressure. The averages are shown as solid lines and the standard deviations of 50 repetitions are shown as the shaded regions. All the injection events show the coolant temperature of 90° C resulted in a slightly longer injection event than the lower temperature conditions. The other portions of the injection event were very similar, with similar opening profiles and similar overall behavior for much of the event. Two methods were used to determine the mass difference between the injection events at different coolant temperatures. The first considers the additional time of injection multiplied by the average or representative injection rate. In Fig. 4 the higher coolant temperature resulted in a ~ 120 μs longer injection event, corresponding to about ~ 1.5 mg more fuel injected compared with the lower temperature condition. The second method is a mathematical integration of the injection rate data. The mathematical integration showed a difference of ~ 2 mg or 9% between the coolant temperatures. The difference between the values is due to small differences in the injection rate profiles at the different coolant temperatures. The integrated mass for a majority of the conditions tested showed the higher coolant temperature yielded between 1% and 5% more fuel primarily due to longer injection events. For clarity and emphasis, Fig. 4 shows the case with the highest difference in integrated mass. Other examples are provided in Figure A6 in the Appendix.

One explanation for the trend of more mass injected at higher fuel injector temperatures may be related to fuel viscosity. Higher temperatures result in lower viscosity, thus reducing the viscous forces required to close the needle at the end of injection. Salvador et al. [25] noticed the same behavior with diesel fuel for multiple injection durations and injection pressures using a solenoid injector. Salvador et al. [25] concluded that higher viscous forces at lower temperatures reduce the maximum needle lift, such that the needle closes from a lower position at

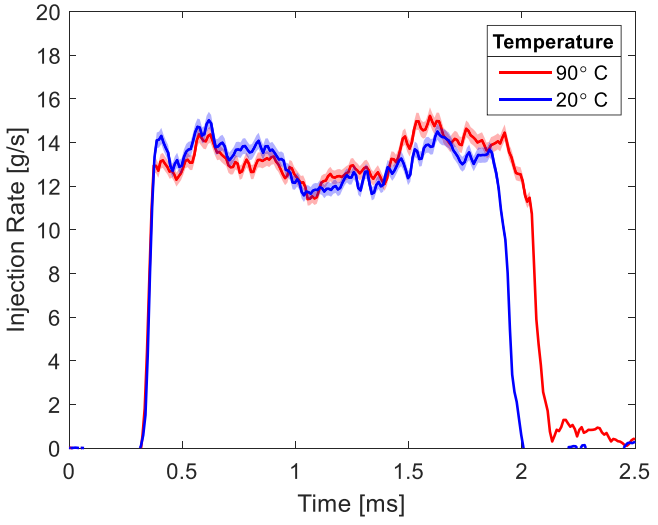

Fig. 4. Average fuel injection rate for two coolant temperatures for Injector Y Holes 1 and 2 at 1500 bar injection pressure and 20 bar chamber pressure.

lower temperatures. This reduces the time needed to close the injector. Guangxin et al. [35] reported similar behavior with dimethyl ether and increasing fuel temperature, attributing the extended injection duration at higher temperatures to changes in fuel properties. Another factor that may affect injection rate is the mechanical operation of the solenoid actuator similar to the temperature effects on piezoelectric driven injectors [36–38]. Both fuel properties and mechanical operation may impact the injection duration.

€

The effects of chamber pressure on injection rate were also investigated. The results show the injection rate was similar for the three chamber pressures of 10, 20, and 30 bar with significant differences only occurring during the injector opening events. See Figure A7 of the Appendix for typical results. Lower chamber pressure exhibited a spike in injection rate during the opening event (with overshoots of a factor of 1.2 to 1.4), particularly at higher injection pressures. This behavior may be due to the limit of the dynamic response of the IRDCI; where the lowest rated pressure for the facility is 10 bar suggesting higher uncertainty and noise in the measurement at lower chamber pressures. Excluding the variation at the start of injection, the results show chamber pressure has minor to negligible effects on injector rate, which is consistent with previous studies of other fuels and injectors [24,39].

The effects of injection pressure on injection rate were consisted with expectations based on previous studies in the literature. Typical results are presented in the Appendix in Figure A8. Increasing fuel injection pressure increased the fuel mass flow rate for the same injection timing due to higher flow velocities. In addition, higher injection pressures resulted in slightly earlier end of injection. This trend was consistent across chamber pressures and the injectors tested at lower coolant temperatures. However, when the coolant temperature was increased to 90° C, the needle opening and closing events were almost identical for most conditions. This trend may be attributable to the fuel viscosity or mechanical operation of the solenoid actuator as discussed earlier. However, there was one exception for the data at higher coolant temperatures for Injector Y at an injection pressure of 600 bar. At these conditions, the mass flow rate data indicate later needle closing.

The hydraulic parameters for each nozzle were determined from the mass flow rate and momentum flux measurements. The characteristic value for each measurement was used for the analysis to determine the momentum coefficient, discharge coefficient, effective area, and effective outlet velocity. The discharge coefficient, C_d, was calculated according to Equation (1) using the measured, $\dot{m}$, and the theoretical, $\dot{m}_t$, mass flow rates. All the coefficients were derived from first principles, and additional details and assumptions are provided in the references [28].

$$C_d = \frac{A_{eff}\rho_f U_{eff}}{A_o \rho_f U_t} = \frac{\dot{m}}{\dot{m}_t} = \frac{\dot{m}}{A_o\sqrt{2\rho_f \Delta P}} \tag{1}$$

where A_o is the outlet area,$A_{eff}$is the effective area,U_{eff} is the effective velocity, U_t is the theoretical velocity, ρ_f is density of the fluid, and ΔP is the difference between fuel injection pressure and chamber pressure.

Fig. 5 presents the ROI results for both injectors tested at 90° C for all injection and chamber pressures as a function of $(\triangle P)^{½}$. The data show, as expected based on Bernoulli's approximation for flow velocity (Equation (1)), that ROI is linearly proportional to $(\triangle P)^{½}$ and that Injector Y consistently produced a higher mass flow rate compared with Injector X. The differences between Injector X and Injector Y are the conicity, inlet hole rounding of the nozzles and nozzle diameters. Injector X has two cylindrical nozzles, one with a slightly larger diameter and one with a slightly smaller diameter than the nozzles of Injector Y. The total physical nozzle outlet diameter (and therefore total nozzle outlet area) for each injector is the same. So the trends may be attributed to the effects of rounding the nozzle inlet (Injector Y) and uniform (Injector X) versus converging/diverging nozzle channel (Injector Y). The mass flow rates for Injector X were consistently lower than the mass

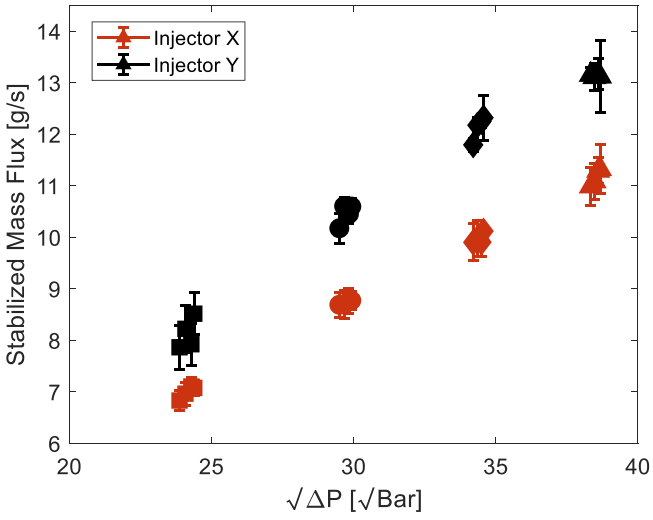

Fig. 5. Characteristic mass flux results for 90° C coolant temperature. The error bars represent the variability in the time interval selected for the characteristic value.

flow rates of Injector Y, by 11% to 22%, with the smallest difference observed at injection pressures of 600 bar and the highest difference observed at injection pressures of 1200 bar. The results indicate rounding has a measurable impact on mass flow rate. Recall, hydro-erosion increases the static flow rate by rounding the nozzle inlet edges. The percentage of hydro-erosion rounding listed in Table 1 is the percent increase in the static flow rate. However, the increase in measured mass flow rate is less than the increase in static flow rate that can be attributed to conicity effects for the orifices of Injector Y.

The discharge coefficient as a function of Reynolds number for both injectors tested at 90° C for all injection and chamber pressures is shown in Fig. 6. Injector Y has consistently higher discharge coefficients, by 24% to 37%, compared with Injector X for all tested conditions. The increased discharge coefficient is attributed to the rounded nozzle inlet edges in Injector Y. Injector X shows a relatively constant discharge coefficient at all Reynolds numbers, which could be an indication of cavitation [28,40–42]; however, Injector Y is also likely cavitating (discussed further below) and shows some sensitivity of the discharge coefficient to Reynolds number. Thus, there are likely additional factors affecting C_d for the injectors.

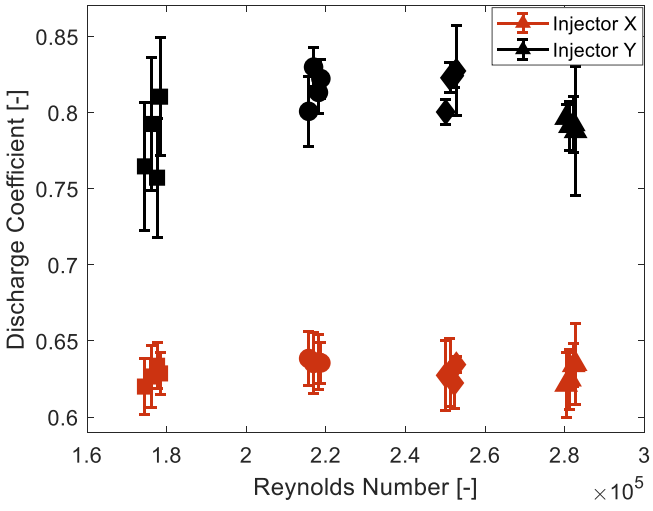

Fig. 6. Discharge coefficient results for 90° C coolant temperature. The error bars represent the variability in the time interval selected for the characteristic value.

5. Momentum flux

The results for momentum flux for chamber pressures of 5 to 30 bar were virtually identical for all chamber pressures, which is consistent with expectations based on the theory and principles used to design the facility [28]. Briefly, as long as the sensor is placed a reasonable distance from the orifice and orthogonal to the spray, the momentum of the jet is unaffected by the chamber density. Increasing injection pressure resulted in an increase in momentum flux, and higher variability in the momentum measurement was observed for higher chamber pressures for all injection pressures. Higher variability may be due to larger flow instabilities such as cavitation at higher injection pressures and partial gas diffusion at higher chamber pressures. Typical momentum flux time-history data are provided in the Appendix for reference (Figs. A9 and A10).

Fig. 7 presents the results for the characteristic momentum flux measurements as a function of △P, and, like the mass flow rate measurements, the results show linear dependence. Here the momentum flux data are resolved to the level of the individual nozzles of the injectors. Injector X Hole 2, with the largest outlet diameter, resulted in the highest momentum flux at all test conditions. At the opposite end of the spectrum, Injector X Hole 1, with the smallest outlet diameter, resulted in the smallest momentum flux at all test conditions. The intermediate results for Injector Y Holes 1 and 2, were close to the values for the largest nozzle diameter, Injector X Hole 2. On average the difference between the nozzles with the highest momentum flux, Injector X Hole 2 and Injector Y Hole 2, is 6%. Between Injector Y Holes 1 and 2, the differences ranged between 7 and 9% for all conditions. Injector Y Holes 1 and 2 have the same outlet diameter but, differ in conicity. Injector Y Hole 2 has a converging nozzle resulting in higher outlet velocities compared with Injector Y Hole 1, which is reflected in the momentum flux data. Overall, the trends indicate the size of the nozzle outlet diameter has a stronger effect on momentum flux than conicity or hydro-erosion rounding.

The theoretical momentum flux can be calculated using △P and the Bernoulli principle for comparison with the experimental data. The ratio between the measured momentum flux, $\dot{M}$, and theoretical momentum flux, $\dot{M}_t$, can then be calculated to obtain the momentum coefficient, C_M, for each nozzle similar:

$$C_M = \frac{A_{eff}\rho U_{eff}^2}{A_o \rho U_t^2} = \frac{\dot{M}}{\dot{M}_t} = \frac{\dot{M}}{2A_o \Delta P} \tag{2}$$

The momentum coefficient results are shown in Fig. 8 for the four orifices. Two trends are observed. The first is the relative performance of the different injector geometries. The nozzles with hydro-erosion rounding (Injector Y) yielded systematically higher momentum coefficients. Hydro-erosion rounding is used to reduce the amount of flow separation and increase the effective area, and the results show rounding does improve nozzle performance, more closely approximating the theoretical value. Injector Y Holes 1 and 2 have the same outlet diameters, but with diverging and converging nozzle passages, respectively. The data show the larger inlet diameter associated with the converging nozzle of Injector Y Hole 2 further reduces flow separation compared with the diverging nozzle. The uniform cross-section/cylindrical nozzles both exhibited lower momentum coefficients, which is attributed to increased flow separation or reduced effective area.

The data also show the momentum coefficient is independent of Reynolds number. Under cavitating conditions, the discharge coefficient only depends on the cavitation number and not on Reynolds number [28,40,41], as shown in Equation (3):

$$C_d = C_c\sqrt{K} = \frac{C_M}{C_v} \tag{3}$$

where K is cavitation number, C_c is the contraction coefficient and C_v is the velocity coefficient. Although some of the nozzle geometries included features to reduce the probability of cavitation, such as the hydro-erosion rounding of the nozzle inlet, all nozzles exhibited this behavior at 90° C coolant temperature. The fuel properties of gasoline combined with the trends observed with the momentum coefficient as a function of high Reynolds number support the conclusion that the nozzle flows experience cavitation.

Fig. 9 shows the momentum coefficient as a function of cavitation number for the four orifices, where the cavitation number is defined based on the study by Nurick [41]. All four orifices show a decreasing trend in momentum coefficient with increasing cavitation number. Several studies have suggested that once cavitation starts, the discharge coefficient is only dependent on cavitation number and essentially independent of Reynolds number [28,41,43,44]. The same studies state that large cavitation numbers suggest non-cavitating flow while small cavitation numbers (close to 1) correspond to strong cavitating flow. The prior discussions are with respect to the discharge coefficient, and Fig. 9 shows the momentum coefficient. However, the discharge coefficient and the momentum coefficient are linearly dependent, as shown in Equation (3), suggesting that under cavitating conditions, the

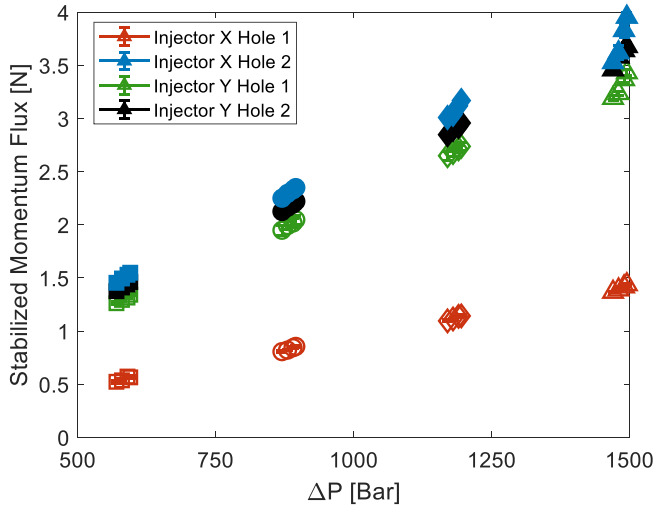

Fig. 7. Characteristic momentum flux results for 90° C coolant temperature. The error bars are smaller than the symbols and they represent the variability in the time interval selected for the characteristic value.

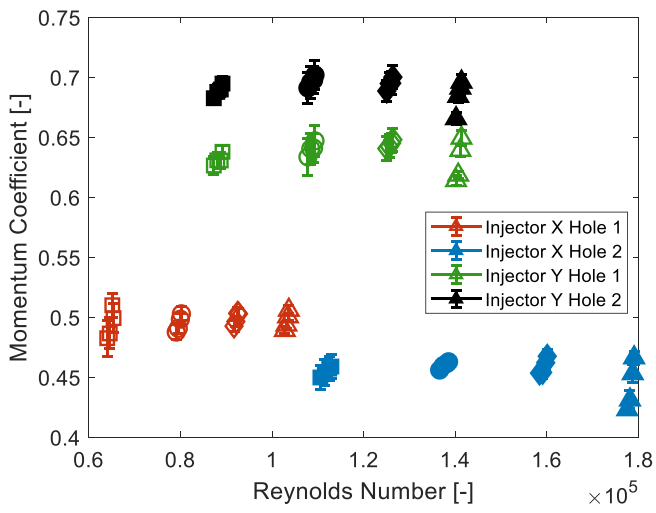

Fig. 8. Momentum coefficient results for 90° C coolant temperature. The error bars represent the variability in the time interval selected for the characteristic value.

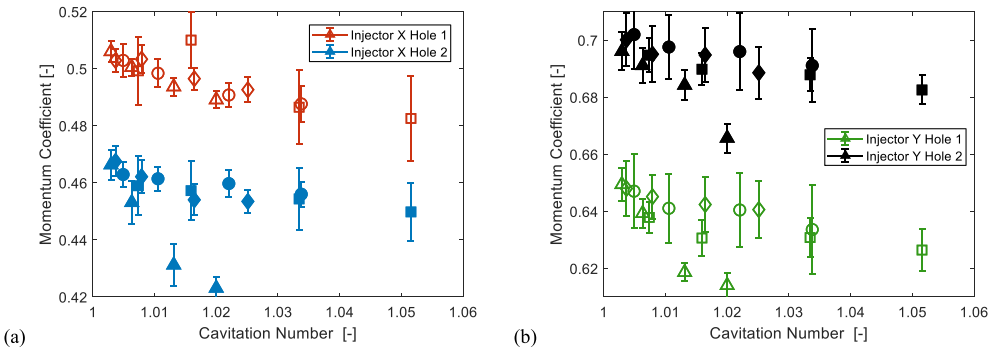

Fig. 9. Momentum coefficient results for the four orifices of (a) Injector X and (b) Injector Y for 90° C coolant temperature. The error bars represent the variability in the time interval selected for the characteristic value.

momentum coefficient is a function of the cavitation number.

External spray features such as spray flutter observed and discussed in Medina et al. [23] using the same injectors support the conclusion that the flow was cavitating. Spray flutter was suspected to be a product of surface roughness, machining defects and/or cavitation. Cavitation was considered more likely due to the fuel volatility and the operating conditions. Thus, several observations indicate the flow is cavitating at all operating conditions for all orifices. To summarize, the downstream external spray features such as spray flutter [23], the cavitation numbers close to 1, the fuel properties, and the negative trend of momentum coefficient with increasing cavitation number all suggest that the nozzles are experiencing cavitation. This is an important conclusion that should be considered when interpreting the other spray measurements and when considering injector design for high-pressure gasoline sprays.

6. Visual spray development

Several chamber temperatures and pressures were tested resulting in 12 total combinations and nine unique chamber densities from 2.11 to 25.27 kg/m^3. Three chamber densities were repeated but, using a combination of different chamber conditions. Fig. 10a shows the average penetration distance for Injector X Hole 1 at 1500 bar injection pressure and 90° C coolant temperature for the 12 chamber conditions. Since the results are based on schlieren imaging, the data include the vapor- and liquid-phase regions of the fuel spray. The data in Fig. 10a are averages of 20 repetitions with error bars representing one standard

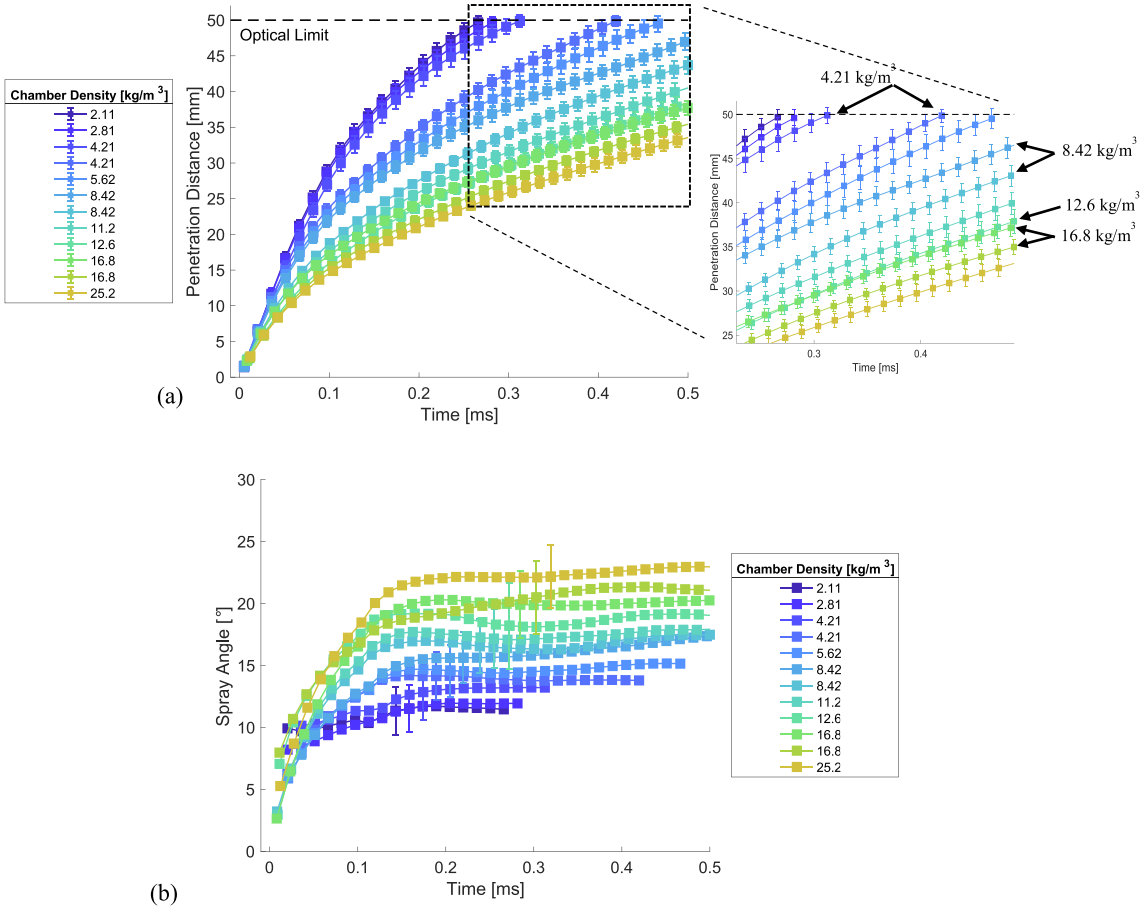

Fig. 10. (a) Average penetration distance and (b) average spray angle for Injector X Hole 1 at 1500 bar injection pressure and 90° C coolant temperature. The error bars are the standard deviation of 20 measurements.

deviation. In the figure, the data are clustered in three groupings with similar penetration behavior. The groupings are due to the different chamber pressures. The fastest penetration data are from the experiments with 5 bar chamber pressure. The slowest penetration data are from the highest chamber pressures of 20 and 30 bar. The smaller differences in the penetration distances within each group are due to the different chamber temperatures. Amongst the same chamber pressure group, the highest temperature results in the fastest penetration due to the lower chamber density. Interestingly, the penetration and spray angle data from the three identical pairs of densities differ (4.21, 8.42 and 16.9 kg/m^3), as seen in Fig. 10a. The trend shows the chamber pressure has a stronger effect on spray penetration distance than chamber temperature, particularly for lower chamber pressures. Also interesting is that for portions of the penetration distance time histories the data for 12.6 and 16.9 kg/m^3 were identical, as seen in the inset of Fig. 10a. All these trends, with respect to the chamber density, chamber pressure and temperature, and the similar penetration data for 12.6 and 16.9 kg/m^3, were observed to some degree for all nozzles and all injection pressures.

The spray angle data presented in Fig. 10b follow a trend of increasing spray angle with increasing chamber density. All conditions exhibited the general behavior of increasing the spray angle rapidly at early times (less than0.1 ms) and then transitioning to a fairly constant spray angle at later times. As with the penetration data, the spray angle data for the three identical densities differ slightly, with the differences being slightly more pronounced at later times. Again, this may indicate chamber pressure is a larger factor on spray development compared with chamber density.

At lower injection pressures, the groupings of data were more pronounced, with greater division between the penetration distances, as seen in Fig. 11 for Injector Y Hole 1 at 600 bar injection pressure. The effects of temperature were smaller at lower chamber pressures, with more overlapping data. However, small differences were still observed between identical chamber densities.

The grouping of the results observed in Figs. 10a and 11 could be a product of the fuel properties that were studied. For example, Payri et al. [5] studied the spray characteristics of n-dodecane and n-heptane in a constant pressure flow reactor and reported that for the same chamber density, a change of 200 K in chamber temperature did not result in any difference in the penetration distance data. However, Naber and Siebers [3] studied diesel spray characteristics in a constant volume chamber at various chamber conditions and reported that for the same chamber density, increasing chamber temperature resulted in reduced penetration distance. The diesel spray characteristics of penetration distance for the same density are similar to the trends observed in this work with gasoline. Both diesel and gasoline are multicomponent fuels while the fuels studied in Payri et al. [5] were single component fuels. Comparing the results of the different studies indicates fuel composition and associated thermophysical properties affect the spray characteristics sufficiently to visibly impact spray penetration.

Several correlations have been previously developed for diesel and gasoline fuel sprays. Of the correlations developed for high fuel injection pressures, the work by Naber and Siebers [3] was selected for comparison here. As noted earlier, the correlation by Tian et al. [21] for high pressure gasoline sprays does not include two phases of spray development and did not agree well with the previous study of high-pressure gasoline sprays by Medina et al. [22]. Naber and Siebers derived a correlation for penetration distance as a function of time based on first principles and the properties of diesel fuel sprays. The correlation is compared with the experimental data from the current work in Fig. 12. In the figure, one panel compares data at the same chamber density, but with different chamber temperatures and pressures, and the other panel compares results from two different chamber densities. The difference between the predictions for the same density is less than 1 mm at each time step, and the difference between the experimental data sets for the same density is less than 4 mm. The diesel correlation predicts very similar penetration curves for the same density while the data shows some differences. The inverse is true for Fig. 12b, where both experimental data are different densities but identical penetration curves. The diesel correlation shows a difference of at least 3 mm. In spite of the differences, both panels show very good agreement between the experimental data and the diesel spray correlation for the entire time intervals (within ~ 8% throughout the time histories).

7. Conclusions

Three methods were used to measure mass flow rate, momentum flux and spray development of high-pressure gasoline fuel sprays using different internal nozzle geometries at a broad range of operating and experimental conditions. The major conclusions based on the results of the study are:

- Internal injector geometry played a considerable role on internal flow dynamics and hydraulic behavior. The mass injection data showed hydro-erosion rounding and conicity increased the mass flow rate between 11 and 22% compared with cylindrical/uniform cross-section nozzles. The momentum data showed larger nozzle diameters and converging and rounded inlet nozzles could be used to achieve similar momentum fluxes, with differences of between 5 and 7% in momentum flux between these two nozzle geometries.
- The combination of data showed all nozzles were cavitating, regardless of injector temperature, nozzle geometry, chamber

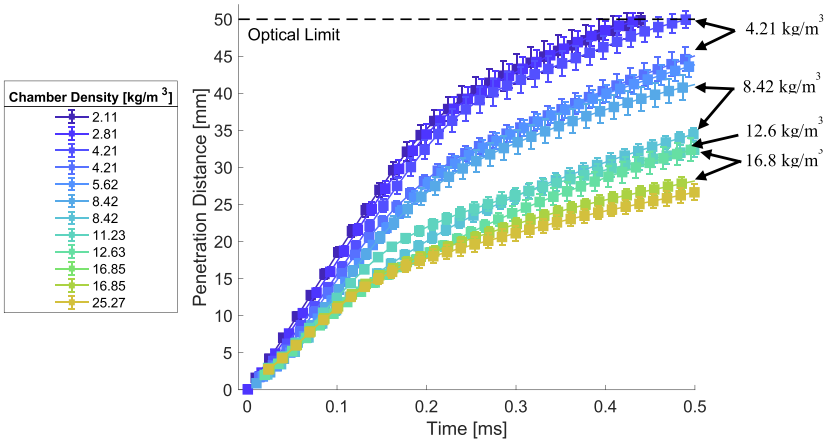

Fig. 11. Average penetration distance for Injector Y Hole 1 at 600 bar injection pressure and 90° C coolant temperature. The error bars are the standard deviation of 20 measurements.

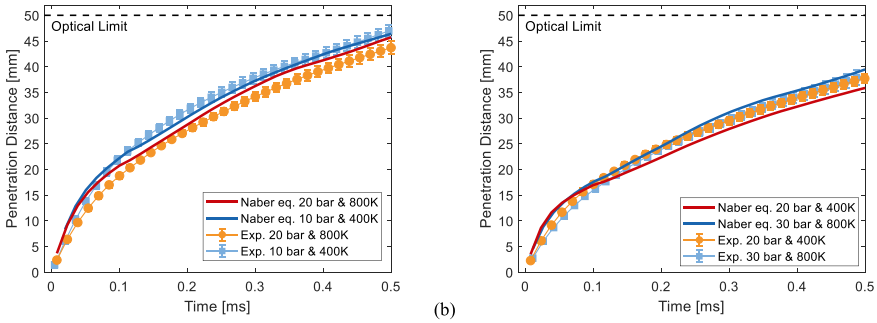

Fig. 12. Comparison of experimental results for Injector X Hole 1 with the spray correlation by Naber and Siebers [3] for (a) chamber density of 8.42 kg/m^3 and injection pressure of 1500 bar and (b) chamber density of 12.6 kg/m^3 and 16.8 kg/m^3.

pressure and injection pressure, as determined by the observed trends for momentum coefficient. Cavitation could be a cause of component damage and can affect fuel flow rates, mixing and atomization.

- Injector temperature had a noticeable effect on the injection rate. Temperature is suspected to affect fuel viscosity and mechanical operation of the injector impacting needle opening and closing events. For a majority of the cases, higher coolant temperature led to 1% to 5% more fuel injected per event.
- In agreement with previous spray visualization studies, chamber pressure had a strong effect on spray penetration, more so than chamber temperature, and the combined parameter of chamber density.
- While nozzle geometry had no effect on the early portion of the spray development, nozzle geometry significantly influenced spray development at later times (e.g., after the spray break-up time), producing similar trends as those observed with the momentum flux measurements.

Declaration of Competing Interest

The authors declare that they have no known competing financial interests or personal relationships that could have appeared to influence the work reported in this paper.

Acknowledgements

The authors would like to acknowledge the generous support of the Mechanical Engineering Department and the Rackham Graduate School at the University of Michigan. The work was also made possible through collaboration with the Engine Research Division, Centro Motores Termicos at Universitat Politecnica de Valencia. We would like to offer special thanks to the faculty, technicians and graduate students at Universitat Politecnica de Valencia that contributed their time and expertise to the work.

Appendix A. Supplementary data

Supplementary data to this article can be found online at https://doi.org/10.1016/j.fuel.2021.120468.

References

[1] Dec JE. A Conceptual Model of DI Diesel Combustion Based on Laser-Sheet Imaging*. SAE Tech. Pap.; 1997. https://doi.org/10.4271/970873.
[2] Hiroyasu H, Arai M. Structure of Fuel Sprays in Diesel Engines. SAE Tech Pap 1990. https://doi.org/10.4271/900475.
[3] Naber J, Siebers DL. Effects of Gas Density and Vaporization on Penetration and Dispersion of Diesel Sprays. SAE Tech Pap 1996. https://doi.org/10.4271/960034.
[4] Taşkiran ÖO, Ergeneman M. Experimental Study on Diesel Spray Characteristics and Autoignition Process. J Combust 2011;2011:1–20. https://doi.org/10.1155/2011/528126.
[5] Payri R, Viera JP, Gopalakrishnan V, Szymkowicz PG. The effect of nozzle geometry over internal flow and spray formation for three different fuels. Fuel 2016;183:20–33. https://doi.org/10.1016/j.fuel.2016.06.041.
[6] Payri R, Gimeno J, Bracho G, Vaquerizo D. Study of liquid and vapor phase behavior on Diesel sprays for heavy duty engine nozzles. Appl Therm Eng 2016;107:365–78. https://doi.org/10.1016/j.applthermaleng.2016.06.159.
[7] Yao C, Geng P, Yin Z, Hu J, Chen D, Ju Y. Impacts of nozzle geometry on spray combustion of high pressure common rail injectors in a constant volume combustion chamber. Fuel 2016;179:235–45. https://doi.org/10.1016/j.fuel.2016.03.097.
[8] Eagle EW, Morris SB, Wooldridge M. High-speed imaging of transient diesel spray behavior during high pressure injection of a multi-hole fuel injector. Fuel 2014;116:299–309. https://doi.org/10.1016/j.fuel.2013.07.120.
[9] Desantes JM, Payri R, Salvador FJ, De la Morena J. Influence of cavitation phenomenon on primary break-up and spray behavior at stationary conditions. Fuel 2010;89(10):3033–41. https://doi.org/10.1016/j.fuel.2010.06.004.
[10] Skeen SA, Manin J, Pickett LM. Simultaneous formaldehyde PLIF and high-speed schlieren imaging for ignition visualization in high-pressure spray flames. Proc Combust Inst 2015;35(3):3167–74. https://doi.org/10.1016/j.proci.2014.06.040.
[11] Cancino LR, da Silva A, De Toni AR, Fikri M, Oliveira AAM, Schulz C, et al. A six-compound, high performance gasoline surrogate for internal combustion engines: Experimental and numerical study of autoignition using high-pressure shock tubes. Fuel 2020;261:116439. https://doi.org/10.1016/j.fuel.2019.116439.
[12] Xuan T, EL-Seesy AI, Mi Y, Lu P, Zhong W, He Z, et al. Effects of an injector cooling jacket on combustion characteristics of compressed-ignition sprays with a gasoline-hydrogenated catalytic biodiesel blend. Fuel 2020;276:117947. https://doi.org/10.1016/j.fuel.2020.117947.
[13] Du J, Mohan B, Sim J, Fang T, Roberts WL. Macroscopic non-reacting spray characterization of gasoline compression ignition fuels in a constant volume chamber. Fuel 2019;255:115818. https://doi.org/10.1016/j.fuel.2019.115818.
[14] Eitel F, Schäfer J, Redante E, Nolte R, Königstein A, Heeger C. Potential and Challenges of Fuel Injection Pressure up to 50 MPa for Gasoline Direct Injection Engines. 26th Aachen Colloq Automob Engine Technol 2017, 2017,:489–508.
[15] Yamaguchi A, Koopmans L, Helmantel A, Karrholm FP, Dahlander P. Spray Characterization of Gasoline Direct Injection Sprays Under Fuel Injection Pressures up to 150 MPa with Different Nozzle Geometries. SAE Tech Pap Ser 2019;1:1–14. https://doi.org/10.4271/2019-01-0063.
[16] Singh R, Han T, Fatouraie M, Mansfield A, Wooldridge M, Boehman A. Influence of fuel injection strategies on efficiency and particulate emissions of gasoline and ethanol blends in a turbocharged multi-cylinder direct injection engine. Int J Engine Res 2021;22(1):152–64. https://doi.org/10.1177/1468087419838393.
[17] Su J, Xu M, Yin P, Gao Yi, Hung D. Particle Number Emissions Reduction Using Multiple Injection Strategies in a Boosted Spark-Ignition Direct-Injection (SIDI) Gasoline Engine. SAE Int J Engines 2015;8(1):20–9. https://doi.org/10.4271/2014-01-2845.
[18] Whitaker P, Kapus P, Ogris M, Hollerer P. Measures to Reduce Particulate Emissions from Gasoline DI engines. SAE Int J Engines 2011;4(1):1498–512. https://doi.org/10.4271/2011-01-1219.
[19] Kim K, Kim D, Jung Y, Bae C. Spray and combustion characteristics of gasoline and diesel in a direct injection compression ignition engine. Fuel 2013;109:616–26. https://doi.org/10.1016/j.fuel.2013.02.060.
[20] Payri R, Garcia A, Domenech V, Durrett R, Plazas AH. An experimental study of gasoline effects on injection rate, momentum flux and spray characteristics using a common rail diesel injection system. Fuel 2012;97:390–9. https://doi.org/10.1016/j.fuel.2011.11.065.
[21] Tian J, Zhao M, Long W, Nishida K, Fujikawa T, Zhang W. Experimental study on spray characteristics under ultra-high injection pressure for DISI engines. Fuel 2016;186:365–74. https://doi.org/10.1016/j.fuel.2016.08.086.
[22] Medina M, Fatouraie M, Wooldridge M. High-Speed Imaging Studies of Gasoline Fuel Sprays at Fuel Injection Pressures from 300 to 1500 bar. SAE Tech Pap 2018. https://doi.org/10.4271/2018-01-0294. c:1–18.
[23] Medina M, Zhou Y, Fatouraie M, Wooldridge M. High-Speed Imaging Study on the Effects of Internal Geometry on High-Pressure Gasoline Sprays. SAE Tech Pap 2020. https://doi.org/10.4271/2020-01-2111.

[24] Bosch W. The Fuel Rate Indicator: A New Measuring Instrument For Display of the Characteristics of Individual Injection. SAE Tech Pap Ser 1968:1. https://doi.org/10.4271/660749.
[25] Salvador FJ, Gimeno J, Carreres M, Crialesi-Esposito M. Fuel temperature influence on the performance of a last generation common-rail diesel ballistic injector. Part I: Experimental mass flow rate measurements and discussion. Energy Convers Manag 2016;114:364–75. https://doi.org/10.1016/j.enconman.2016.02.042.
[26] Payri R, Gimeno J, Martí-Aldaraví P, Viera A. Measurements of the mass allocation for multiple injection strategies using the rate of injection and momentum flux signals. Int J Engine Res 2020. https://doi.org/10.1177/1468087419894854.
[27] Payri R, Salvador FJ, Gimeno J, Bracho G. A new methodology for correcting the signal cumulative phenomenon on injection rate measurements. Exp Tech 2008;32(1):46–9. https://doi.org/10.1111/ext.2008.32.issue-110.1111/j.1747-1567.2007.00188.x.
[28] PAYRI R, GARCIA J, SALVADOR F, GIMENO J. Using spray momentum flux measurements to understand the influence of diesel nozzle geometry on spray characteristics. Fuel 2005;84(5):551–61. https://doi.org/10.1016/j.fuel.2004.10.009.
[29] Payri R, García-Oliver JM, Bardi M, Manin J. Fuel temperature influence on diesel sprays in inert and reacting conditions. Appl Therm Eng 2012;35:185–95. https://doi.org/10.1016/j.applthermaleng.2011.10.027.
[30] Meijer M, Somers B, Johnson J, Naber J, Lee S-Y, Malbec LM, et al. Engine Combustion Network (ECN): Characterization and comparison of boundary conditions for different combustion vessels. At Sprays 2012;22(9):777–806. https://doi.org/10.1615/AtomizSpr.v22.i910.1615/AtomizSpr.2012006083.
[31] Parrish SE. Evaluation of Liquid and Vapor Penetration of Sprays from a Multi-Hole Gasoline Fuel Injector Operating Under Engine-Like Conditions. SAE Tech Pap 2014;7(2):1017–33. https://doi.org/10.4271/2014-01-1409.
[32] Pastor JV, Payri R, Garcia-oliver JM, Nerva J. Schlieren Measurements of the ECN-Spray A Penetration under Inert and Reacting Conditions. SAE Int 2012. https://doi.org/10.4271/2012-01-0456.
[33] Payri R, Salvador FJ, Bracho G, Viera A. Differences between single and double-pass schlieren imaging on diesel vapor spray characteristics. Appl Therm Eng 2017;125:220–31. https://doi.org/10.1016/j.applthermaleng.2017.06.140.
[34] Benajes J, Payri R, Molina S, Soare V. Investigation of the influence of injection rate shaping on the spray characteristics in a diesel common rail system equipped with a piston amplifier. J Fluids Eng Trans ASME 2005;127:1102–10. https://doi.org/10.1115/1.2062767.
[35] Guangxin G, Zhulin Y, Apeng Z, Shenghua L, Yanju W. Effects of Fuel Temperature on Injection Process and Combustion of Dimethyl Ether Engine. J Energy Resour Technol 2013;135:1–5. https://doi.org/10.1115/1.4023549.
[36] Payri R, Gimeno J, Mata C, Viera A. Rate of injection measurements of a direct-acting piezoelectric injector for different operating temperatures. Energy Convers Manag 2017;154:387–93. https://doi.org/10.1016/j.enconman.2017.11.029.
[37] Mitrovic M, P. Carman G, K. Straub F. Response of piezoelectric stack actuators under combined electro-mechanical loading. Int J Solids Struct 2001;38(24-25):4357–74. https://doi.org/10.1016/S0020-7683(00)00273-0.
[38] Ferrari A, Mittica A. FEM modeling of the piezoelectric driving system in the design of direct-acting diesel injectors. Appl Energy 2012;99:471–83. https://doi.org/10.1016/j.apenergy.2012.05.048.
[39] Payri R, Gimeno J, Marti-aldaravi P, Vaquerizo D. Internal Flow Characterization on an ECN Injector. At Sprays 2015;26:889–919. https://doi.org/10.1615/atomizspr.2015013930.
[40] Benajes J, Pastor JV, Payri R, Plazas AH. Analysis of the Influence of Diesel Nozzle Geometry in the Injection Rate Characteristic. J Fluids Eng 2004;126:63. https://doi.org/10.1115/1.1637636.
[41] Nurick WH. Orifice cavitation and its effect on spray mixing. J Fluids Eng Trans ASME 1977;99:426–7. https://doi.org/10.1115/1.3448785.
[42] Payri R, Gimeno J, Cuisano J, Arco J. Hydraulic characterization of diesel engine single-hole injectors. Fuel 2016;180:357–66. https://doi.org/10.1016/j.fuel.2016.03.083.
[43] Sun Y, Guan Z, Hooman K. Cavitation in Diesel Fuel Injector Nozzles and its Influence on Atomization and Spray. Chem Eng Technol 2019;42(1):6–29. https://doi.org/10.1002/ceat.v42.110.1002/ceat.201800323.
[44] He Z, Guo G, Tao X, Zhong W, Leng X, Wang Q. Study of the effect of nozzle hole shape on internal flow and spray characteristics. Int Commun Heat Mass Transf 2016;71:1–8. https://doi.org/10.1016/j.icheatmasstransfer.2015.12.002.